PASJ: Publ. Astron. Soc. Japan **50**, 375–387 (1998)

A Hybrid N-Body/Cellular Automaton Scheme for Modelling Propagating Star Formation in Galaxies

Lance T. GARDINER
Department of International Education, Sun Moon University, Tangjeongmyeon, Asan-kun, Chung-nam, 336-840 Republic of Korea
E-mail (LTG): ltg@omega.sunmoon.ac.kr

Colin TURFUS
Department of Mathematics, Sun Moon University, Tangjeongmyeon, Asan-kun, Chung-nam, 336-840 Republic of Korea
and
Meishing WANG
Chonan Campus Computer Centre, Sun Moon University, Samyong-dong, Chonan-si, Chung-nam, 330-150 Republic of Korea

(Received 1998 February 16; accepted 1998 June 16)

Abstract

We present a numerical scheme for modelling star formation in galaxies based on the dual operation of gravitational instabilities and propagating star formation. Star formation is superposed on a mechanical N-body simulation of a collisional particle system by using a cellular automaton framework. The simulations involve 5000 particles representing gas clouds which can collide inelastically, and have been performed on a 2D square surface with quasiperiodic boundary conditions. The input of kinetic energy from star-forming regions leads to self-regulation of the global dynamics of star formation. The model naturally generates cloud complexes assembled from groups of cloud particles and simulates the ignition and propagation of star formation in such complexes leading to the formation of low density bubbles and expanding shells. The percentage of the model surface undergoing star formation and the ratio of the rates of stimulated to spontaneous star formation are shown to be consistent with models based on the theory of Stochastic Self-Propagating Star Formation (SSPSF). The code is shown to lead to star formation that propagates very nearly isotropically and can thus be adapted to the case of rotating disc galaxies without geometrical modification.

Key words: Galaxies: irregular — Interstellar: clouds — Numerical methods — Stars: formation

1. Introduction

Since the late-1970s, a variety of numerical schemes have been devised for modelling the global spatio-temporal evolution of star formation in galaxies. Star-forming numerical codes have been applied to various problems, including the generation of star-formation patterns in spiral and flocculent galaxies (e.g., Gerola, Seiden 1978; Hausmann, Roberts 1984; Elmegreen, Thomasson 1993; Sleath, Alexander 1995), studies of fluctuations in global rates of star formation in dwarf and irregular galaxies (Gerola et al. 1980; Feitzinger et al. 1981), the effects of interaction between galaxies on star formation (e.g., Kojima, Noguchi 1997; Noguchi, Ishibashi 1986; Noguchi 1988, 1991; Mihos, Hernquist 1994) and the formation of galaxies (e.g., Tissera et al. 1997; Navarro, White 1993). The methodologies employed may be classified into two main camps: (1) the superposition of star formation on a particle-based simulation, and (2) cellular automaton methods. Methods of Type (1) may be further classified into two groups based on the representation of the interstellar medium. The interstellar medium is considered either (a) to be represented by discrete inelastic clouds ('sticky-particle' methods), or (b) to comprise a continuous fluid (Smoothed-Particle Hydrodynamical methods). The basic physics included in methods of Type (1) comprises gravitational forces and gas dissipation processes, together with kinetic energy input from newly formed stars. In cellular automaton (CA) methods, time, space, and the physical properties of the medium are all discretized. In star-forming CA schemes, spatial discretization is achieved through performing computations on a 2D grid of cells, while physical properties are represented by integer states (Turfus, Gardiner 1996). The physics is encoded in a set

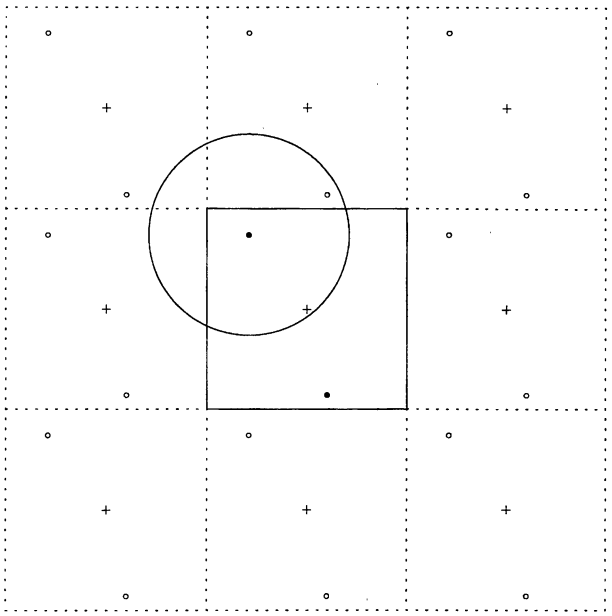

Fig. 1. Schematic representation of the application of quasiperiodic boundary conditions for the gravitational force calculation. The simulation area comprises the central square and the periodic replicas of the simulation area are indicated by dotted lines. The centre of the simulation area (cross), and two particles (filled circles) with their image replicas (open circles) are shown. The force interaction area for one of the particles is indicated by a circle with radius 0.5 LU, which encloses the image replica of the other particle shown.

of rules by which each cell state evolves in accordance with the states of its neighbours. The concept of propagating star formation, by which star formation can spread from cell to cell, could be naturally applied within such a framework. Star formation schemes based on cellular automata implicitly include gravitation through the inclusion of galactic rotation. The simple case of circular orbits in the models of Stochastic Self-Propagating Star Formation (SSPSF) (Gerola, Seiden 1978; Seiden, Gerola 1979) has been modified to allow non-circular velocity fields (Perdang, Lejeune 1996; Lejeune, Perdang 1996).

In this paper, we present a new scheme to model star-formation in galaxies in which the methodologies (1a) and (2) outlined above are combined. The recognition that star formation is fundamentally the result of gravitational processes which are able to produce the required density enhancements leads us to consider an N-body simulation of a system of self-gravitating particles as the foundation for our model. The fluid dynamical analysis of Elmegreen (1989) suggests that gravitational instabilities can operate effectively in a cloudy interstellar medium on a variety of length scales to produce gas cloud complexes. This leads us to consider the particles of our simulation as gas clouds which can collide with each other inelastically, thereby reducing their velocity dispersion and making them susceptible to gravitational agglomeration. Even in the absence of particle self-gravity, clumping of material can occur by random collisional agglomeration; however, the rate of cloud complex formation is much reduced in such a model (see section 5). Our star formation algorithm is based on the application of a cellular automaton to the particle distribution. Two modes of star formation are included: spontaneous and stimulated star formation. The explicit addition of a mechanism for stimulated star formation to an N-body simulation is a novel feature of our numerical scheme. Feedback of kinetic energy into the system is achieved by the boosting of nearby cloud particles by stellar tracer particles representing OB-star associations.

A description of the numerical scheme follows in the next section. In sections 3 and 4, the results of our simulations are presented. Section 3 summarizes the dependence of the simulation results on model parameters and presents analyses of various global properties of the simulations. In section 4, graphical output of the spatio-temporal evolution of the model is presented and reviewed. In section 5, we discuss the relationship of our numerical scheme to simpler models of star formation in galaxies. Section 6 discusses the adaptation of the code to future models of disc galaxies.

2. The Numerical Model

2.1. The Basic Setup

Our simulations are performed on a 2D square surface with periodic boundaries (see figure 1). This represents a somewhat unconventional departure from the usual practice of constructing realistic simulations of rotating disc galaxies, although the use of periodic boundaries is common for N-body cosmological simulations. Our eventual aim is, of course, to apply our numerical scheme to simulate actual disc galaxies and such work is currently in progress. However, the geometry we have adopted here has a number of significant advantages over circular geometry for testing and evaluating a numerical scheme for star formation in galaxies. Our simulations enable us to survey a large domain of the parameter space unprejudiced by restrictions imposed by having to adopt a certain form for the galactic potential with a given initial distribution of matter. Furthermore, analysis of the results is greatly simplified owing to the ease with which the surface area can be divided up into square elements together with the lack of any *a priori* spatial dependence of the properties of the simulation.

The square geometry of our present model, characterized by the absence of any rotation of the system, suggests that it may better illuminate the spatio-temporal

evolution of star formation in irregular galaxies rather than in galaxies with spiral structure for which differential rotation is a key factor. Irregular galaxies are generally smaller and less evolved in terms of chemical enrichment and gas mass fraction. Their slow rates of differential rotation characteristically result in a disorganized optical appearance due to the free-wheeling nature of star formation unforced by spiral density waves. The Large Magellanic Cloud (LMC), a satellite of the Milky Way at a distance of about 50 kpc, is one of the closest external galaxies and by far the most well studied irregular galaxy. We use the LMC as our benchmark galaxy for choosing various parameters for the model setup as well as for comparing simulation results.

The dimensions of our simulation are chosen to be 5 kpc × 5 kpc, comparable to the area of the LMC within which active star formation is currently taking place (Smith et al. 1987). We take one length unit (LU) to be equivalent to 5000 pc and thus the model has dimensions of 1 LU on each side. Five thousand particles representing discrete gas clouds form the gaseous component in our model system. Each particle has a mass of $6\times10^4\,M_\odot$, giving a total mass of $3\times10^8\,M_\odot$ for the whole system, consistent with the mass of H I gas in the central system of the LMC (Luks, Rohlfs 1992). Our simulation has no stellar component since we assume that the stellar system simply provides a smooth uniform background potential. The only gravitational forces in our model derive from the cloud particles themselves. The timestep used in our simulations was 0.5 Myr, chosen to minimize the fraction of missed collisions between cloud particles (see subsection 2.3).

There are four separate aspects to the simulation code; each of these is coded in a separate FORTRAN subroutine. The basic foundation for the model is the gravitational N-body simulation. The second level involves the handling of inelastic collisions between the cloud particles which reduce their overall kinetic energy. The next level involves the superposition of a 100 × 100 square array on the 2D surface and the application of simple cellular automaton rules to handle star formation. The fourth level involves the radial boosting of neighbouring cloud particles by the stellar tracer particles created in the simulation. Each of these separate aspects is discussed below.

2.2. *The Gravitational N-Body Simulation*

The gravitational force on an individual particle is given by the sum of the force contributions from all particles of the system lying within a finite cutoff radius of 0.5 LU. As shown in figure 1, we perform our computations using a 2D periodic tiled surface, and thus there is no central point analogous to the centre of a real galaxy towards which matter tends to collapse. In this respect, our setup resembles an infinite self-gravitating sheet, but the periodicity prevents the growth of gravitational instabilities with a wavelength exceeding 1 LU. These boundary conditions are similar to the quasiperiodic boundary conditions for cosmological N-body simulations employed by Bouchet and Hernquist (1988), except that a circular force cutoff radius has been used instead of an interaction box having the same dimensions as the simulation. As in the cosmological model, the periodic boundaries in our model allow particles to exit the simulation area and reenter it through the opposing edge.

All model calculations are carried out in a Cartesian (x, y) coordinate system. The force per unit mass applied to an individual particle is given by:

$$\ddot{\boldsymbol{r}}_i = -G \sum_{j\neq i, d<d_{\rm fc}}^{n} \frac{m_j[\boldsymbol{r}_i - (\boldsymbol{r}_j + \boldsymbol{c})]}{[|\boldsymbol{r}_i - (\boldsymbol{r}_j + \boldsymbol{c})|^2 + \epsilon^2]^{3/2}}, \tag{1}$$

where $\boldsymbol{r}_i$ denotes the position vector of the i-th particle, m_i is the particle mass, and G is the gravitational constant. The added offset due to the periodicity of the surface is denoted by $\boldsymbol{c}$. The individual components of the vector $\boldsymbol{c}$ can only take on values of 0, −1, and 1. There is no force contribution from particles which lie outside the force cutoff radius, $d_{\rm fc} = 0.5$ LU. The softening parameter is denoted by ϵ. The value chosen was $\epsilon = 15$ pc, set equal to the value of the cloud particle radius, $r_{\rm cl}$ (see subsection 2.3).

The force computation is carried out using an adaptation of the tree code algorithm of Barnes and Hut (1986) to the case of a 2D surface with quasiperiodic boundaries and a circular force cutoff radius. It incorporates just three hierarchical tree levels with a maximum cell size equivalent to 0.04 LU. A greater number of hierarchical levels involving larger cell sizes was prohibited by increased errors related to edge effects at the force cutoff radius. As prescribed by the tree code method, a given cell contributes to the total force on a particle only if it satisfies an opening criterion (Dubinski 1996):

$$d > \frac{l}{\theta} + \delta, \tag{2}$$

where l is the distance of the particle from the cell, θ is the opening angle parameter, and δ is the distance between the centre of mass of a cell and its geometric centre. If the opening criterion is not satisfied for any large-size cell (0.04 LU), it is resolved into sixteen smaller subcells (0.01 LU). If any subcell fails to satisfy the opening criterion, the force contributions from individual particles are evaluated directly. The positions and velocities of the cloud particles were evolved forward in time using a second order Runge-Kutta integration scheme with a time step of 0.5 Myr.

An estimate of the accuracy of the gravitational force calculations was obtained using data from acceptable simulation runs as described in subsection 3.1. Employing the definition of the relative error adopted by

Hernquist (1987), a figure of 0.7% was obtained with reference to accelerations derived from a direct sum over all interparticle forces for an opening angle parameter, $\theta = 0.5$. In our present simulations, the net gravitational force per particle comprises a small perturbation superimposed on a nearly uniform background potential. However, for the case of disc galaxies dominated by a central potential, a larger value of θ should give a comparable nominal accuracy. For such models, a greater opening angle parameter combined with the application of a full tree code would result in a significant gain in computational efficiency, thereby permitting the use of larger particle numbers if desired.

2.3. *Collisions between Cloud Particles*

The particles in our simulation represent a clumpy interstellar medium divided up into a number of discrete gas clouds. The gas dynamics of the interstellar medium is simulated by allowing cooling via cloud–cloud collisions which reduce the overall kinetic energy. We use the so-called 'sticky-particle' method (Roberts, Hausmann 1984; Noguchi, Ishibashi 1986), a frequently adopted technique for handling gas dissipation in global star formation and gas-dynamical simulations. In our model, the interstellar medium is represented by 5000 gas clouds each with a finite radius. The adopted radius of the gas clouds, $r_{\rm cl} = 15$ pc, is appropriate for achieving sufficient resolution for the generation of star formation patterns based on a star formation cell size of 50 pc (see subsection 2.4). The mean free path of the gas clouds in our simulation, having typical values for the velocity dispersion, is about 170 pc. Given a total system mass of $3 \times 10^8\, M_\odot$, the mass of each cloud particle is $6 \times 10^4\, M_\odot$.

The 'sticky-particle' method is as follows. If two cloud particles lie within a distance $2r_{\rm cl}$ from each other, their relative velocities along the line joining their centres are reversed and multiplied by an elasticity factor, $f_{\rm col}$. The transverse velocity components of the particles will remain unchanged. The value of $f_{\rm col}$ is a free adjustable parameter in our simulations. The range of values employed was $0.4 < f_{\rm col} < 0.8$. Multiple collisions between particles are included by summing the incremental velocities produced by each single collision. Since our simulations are implemented on a periodic surface, the algorithm also searches for collisions across the model boundaries.

The minimization of the fraction of missed collisions is the primary factor affecting the choice of the time step duration. In practice, the duration of the time step, $t_{\rm step}$, should satisfy (Noguchi, Ishibashi 1986):

$$v_{\rm disp}.t_{\rm step} < r_{\rm cl}, \tag{3}$$

where $v_{\rm disp}$ is the overall systemic velocity dispersion and $r_{\rm cl}$ is the cloud radius. In acceptable simulations (see subsection 3.1), the systemic velocity dispersion is about 16 km s^{-1}. For $r_{\rm cl} = 15$ pc, our adopted time step duration, $t_{\rm step} = 0.5$ Myr, satisfies the above condition.

The duration of our time step ensures that the fraction of missed collisions should be very small for surface number densities of particles comparable to the global mean density. However, the gas cloud complexes which form in our model have surface densities up to about ten times higher than the global mean surface number density. In such crowded areas, the density is so high that the cloud particle radii overlap. Owing to computational limitations, the modelling of the internal dynamics of gas cloud complexes in our simulations is necessarily rather crude, but should be sufficient for describing the gravitational collapse of a core region where star formation can be initiated.

2.4. *Star Formation*

Our model incorporates two modes for the ignition of star formation: spontaneous and stimulated processes. As shown by the theoretical calculations of Elmegreen (1989), self-gravitating cloud complexes can spontaneously form by gravitational instabilities in a clumpy interstellar medium. Loosely bound cloud complexes formed in this way can dissipate their internal kinetic energy and contract to densities high enough to form molecular clouds which will be the birthplace for massive stars. Once star formation is spontaneously initiated, it can propagate through the rest of the cloud complex via the action of H II ionization fronts, stellar winds, and supernovae. These energetic phenomena associated with very young massive stars generate shocks which compress the interstellar medium. In this way, further gravitational instabilities are triggered, leading to the formation of new generations of stars. An account of propagating star formation in LMC Shapley Constellation III is presented by Dopita, Mathewson, and Ford (1985) (see also Domgörgen et al. 1995; Reid et al. 1987).

The initiation of star formation in our model is determined by rules which govern a cellular automaton (CA) covering the model area, but we actually employ a stellar tracer particle generated at each star formation event to represent a newly formed OB-star association. The star formation scheme involves the construction of a CA grid over the 1 LU square model surface by dividing it up into a 100×100 array of 0.01 LU (50 pc) square cells. Although the choice of the cell size is somewhat arbitrary, we mention here that 50 pc is close to the mean value for the size of OB-star associations in the LMC found by Braunsfurth and Feitzinger (1983). The CA has three integer state variables: star formation, s, activity, a, and gas density, n, which are sufficient to determine the ignition and propagation of star formation. The variable n is simply given by the number of cloud particles in the cell; s takes on values of 0 or 1 representing star

formation *off* or *on* determined by the absence ($s = 0$) or presence ($s = 1$) of at least one stellar tracer particle in the cell; a takes on values of 0 or 1 corresponding to an inactive or active state determined by the absence ($a = 0$) or presence ($a = 1$) of at least one stellar tracer particle with an age greater than or equal to 4 time steps in the cell. The distinction between the variables s and a lies in the fact that we allow a period of 4 time steps after the creation of a stellar tracer particle, equivalent to 2 Myr, before it becomes 'active', i.e., capable of propagating star formation and providing kinetic boosts to nearby particles.

The CA rules for the initiation of star formation are applied using periodic boundaries and are stated as follows:

(1) Spontaneous star formation ($s = 0 \rightarrow 1$) is initiated in a cell with state $s = 0$ if $n \geq n_{\rm sp}$, where $n_{\rm sp}$ is the particle number density threshold for *spontaneous* star formation.

(2) Stimulated star formation ($s = 0 \rightarrow 1$) is initiated in a cell with state $s = 0$ if $n \geq n_{\rm st}$ and if at least one of eight cells adjacent to it (i.e., in the 'Moore' neighbourhood) is active, i.e., has $a = 1$. Here, $n_{\rm st}$ is the particle number density threshold for *stimulated* star formation and $n_{\rm st} < n_{\rm sp}$. Both $n_{\rm sp}$ and $n_{\rm st}$ are free adjustable integer parameters.

Once star formation is deemed to occur, a stellar tracer particle is created at a position given by the centre-of-mass of the cloud particles in the cell with the mean velocity of the cloud particles in that cell. The above CA rules imply that only one stellar particle may be formed per cell per time step, and no particles may be formed in a cell already containing a stellar tracer particle ($s = 1$). The stellar tracer particles subsequently move ballistically (i.e., as massless test particles) in the local gravitational field. As well as their positions and velocities, the time since their creation is monitored. As already mentioned, there is an inactive period consisting of 4 time steps after creation. This corresponds to the time required for stars to actually form before releasing energy into the surrounding medium and initiating star formation in neighbouring cells. In practice this sets a limit on the speed of propagation of star formation, given by the cell size divided by the inactive period. The maximum speed of propagation is thus 28 km s^{-1} in the rectilinear direction and 35 km s^{-1} in the diagonal direction. The active period is set to 20 time steps, corresponding to 10 Myr — the approximate life span for a generation of massive stars, so the stellar tracer particle is deleted 24 time steps after its creation.

Our numerical scheme naturally generates gas cloud complexes typically containing $\sim$100–150 individual cloud particles. Such clumping of matter occurs as a result of gravitational agglomeration due to the self-gravity of the particles assisted by dissipation of kinetic energy through inter-particle collisions. Such structures contract under their own self-gravity increasing the central surface density. By applying a number density threshold for spontaneous star formation we can simulate the ignition of star formation at the dense core of the cloud complex. Following the start of star formation in a cell, star formation can propagate into neighbouring cells, which occurs physically via the action of shock waves produced by stellar winds and supernovae. We allow stimulated star formation to occur at a lower threshold density of particles per cell compared to that required for spontaneous star formation since the action of such shock waves should be more efficient in causing the gas to collapse to form stars than in the case of gravity acting alone. The assumption that star formation is more easily stimulated by existing star formation activity than being spontaneously ignited is the fundamental concept upon which models of propagating star formation, including the SSPSF theory, are based.

2.5. *Kinetic Energy Input from Young Massive Stars*

Stellar winds and supernovae produced by young massive stars are highly energetic phenomena resulting in the deposition of large quantities of mechanical energy into the interstellar medium. The localized injection of kinetic energy from such sources counterbalances the global dissipation of kinetic energy via gas cloud collisions and contributes towards maintaining the ergodicity of the system. In a similar way to other star-forming galaxy codes (e.g., Noguchi 1988; Sleath, Alexander 1995), we model the kinetic energy input from young stellar associations by giving cloud particles a radial boost centred on each stellar tracer particle. At each time step, the velocity of a cloud particle lying within a distance r of a stellar tracer particle is increased by an amount, Δv, in the radial direction, given by

$$\Delta v(r) = \begin{cases} v_{\rm bst} \exp\left[1 - \dfrac{1}{1-(r/r_{\rm max})^2}\right], & r \leq r_{\rm max}, \\ 0, & r > r_{\rm max}, \end{cases} \quad (4)$$

where $v_{\rm bst}$ is the maximum boost velocity, a free parameter, and $r_{\rm max}$ is the maximum boost radius, set equal to 50 pc. Only stellar tracer particles older than 4 time steps (i.e., which are 'active' as defined in subsection 2.4), can give a boost to cloud particles. All cloud particles lying within the maximum radius receive a boost, which is also applied across the periodic boundaries of the system. For simplicity, we have taken the boost function to be constant as a function of time until the stellar tracer particle is deleted. We expect that stellar winds from massive young stars are principally responsible for energy deposition in the interstellar medium during the early phase of the evolution of an OB-star association ($T < 3$ Myr) and that supernovae provide the dominant contribution

for the later phase ($3 < T < 10$ Myr) (Bruhweiler et al. 1980).

Our simulations are not constrained to conserve momentum due to the fact that the velocity boosts given by stellar tracer particles can lead to the creation of excess momentum in particular directions if nearby cloud particles are not distributed isotropically with respect to the stellar tracer particles. Simulation results show that drifts in the mean system velocity amounting to between 5 and 10 km s^{-1} can build up over a period of 2000 time steps.

2.6. *Initial Conditions*

Simple random conditions were employed to start up the simulations. A uniform random number generator was used to produce the initial x and y coordinates for the particles. The particles were also given a random initial velocity with a 2D Gaussian distribution having a mean of 0 km s^{-1} and a standard deviation of 10 km s^{-1}. No stellar tracer particles are introduced at the start of the simulation. The simulations were usually run for a period of 2000 time steps with different combinations of the free parameters $f_{\rm col}$, $n_{\rm sp}$, $n_{\rm st}$, and $v_{\rm bst}$, and different starting conditions specified by the seed random number supplied to the random number generator. Each simulation representing 1 Gyr of galactic evolution took around 24 hours of CPU time on a 266 MHz DEC Alpha Workstation. The calculations were performed with double precision accuracy. The simulation data were written to disk every five time steps, and various global system indicators, including the rms velocity dispersion and star formation rate, were computed every time step and recorded.

3. Simulation Results — Global Properties

3.1. *Exploration of the Parameter Space*

Our simulations have only four adjustable free parameters, the elasticity parameter, $f_{\rm col}$, the spontaneous and stimulated star formation thresholds, $n_{\rm sp}$ and $n_{\rm st}$, and the maximum boost velocity $v_{\rm bst}$. The fixed parameters include the size of the model surface, the total mass of the system, the number of cloud particles and their radii, the sizes of the star-forming cells, the form and time dependence of the boost function, and the duration of the time step. Observationally realistic and/or workable values for these latter parameters were chosen as described earlier in section 2.

A large number of simulations were run with various combinations of the four free parameters. The main criterion used for determining whether a particular simulation was acceptable or not was based on the observation that in irregular galaxies typically only a few percent of the surface area is covered with star formation activity as revealed by the existence of H II regions (Hunter 1982). Such galaxies, being without global spiral structure, have a greater resemblance to the non-rotational dynamics of our model. In practice we used the criterion that the mean number of stellar tracer particles per time step, which each represent an area of approximately one star formation cell, should not exceed approximately 5% of the total number of cells in the 100×100 CA array for star formation initiation, i.e., the number of stellar tracer particles per time step should have an average value ≤ 500. An additional criterion is that we require ergodicity of the system. This implies that major system indicators, e.g., the global star formation rate and the mean velocity dispersion of the system, should not have any monotonic increasing or decreasing trends. In practice, it turned out that in all simulations satisfying the mean star formation rate and ergodicity criteria, acceptable star formation structures were generated. Thus, as far as we can discern from our coverage of the parameter space, these two criteria seem to be both necessary and sufficient conditions for acceptable simulations. Acceptable star formation structures are characterized by the formation of gas cloud complexes, ignition and propagation of star formation, and subsequent radial expansion and dissolution of the complexes by the energy input from young stars (see section 4).

In our survey of the parameter space it was found that of the adjustable parameters, the three parameters $f_{\rm col}$, $n_{\rm sp}$, and $n_{\rm st}$ were the major ones determining the global mean star formation rate, whereas $v_{\rm bst}$ did not strongly influence this rate even when adjusted over a fairly wide range. In fact, the values of the three primary parameters can be mutually adjusted to satisfy the acceptability criteria and thus a number of sets of these parameters produced similar simulations in terms of mean star formation rates and star formation morphology. As is to be expected, the effect of increasing (decreasing) the star formation threshold parameters $n_{\rm sp}$ and $n_{\rm st}$ is to make star formation harder (easier) to ignite and propagate leading to a decrease (increase) in the average star formation rate. The elasticity parameter, $f_{\rm col}$, influences the rate at which gas cloud particles can dissipate their kinetic energy and collapse into cloud complexes in which star formation will eventually occur. Hence, increasing (decreasing) the value of $f_{\rm col}$ leads to a decrease (increase) in the overall star formation rate. We found that parameter sets ($f_{\rm col}$, $n_{\rm sp}$, $n_{\rm st}$) given by (0.6, 6, 4), (0.8, 5, 4), and (0.4, 7, 5) could all produce acceptable simulations. The parameter set (0.6, 6, 4) was used for most of our investigations and all the results discussed hereafter refer to simulations conducted with this combination of parameters.

We now turn to the role of the secondary parameter, $v_{\rm bst}$. The effect of increasing the value of $v_{\rm bst}$ is to increase the average (taken over time) rms velocity dispersion of the system after subtracting out the

mean value of the x, y velocity components of all the particles. The following approximate empirical formula was found to hold for the relationship between $v_{\rm bst}$ and the mean rms velocity dispersion, $v_{\rm disp}$, for the range $10 < v_{\rm bst} < 20$ km s^{-1},

$$v_{\rm disp} = 6.0 + 1.02\, v_{\rm bst}, \tag{5}$$

where the velocities are expressed in km s^{-1}. As $v_{\rm bst}$ is reduced, the situation becomes complicated by the onset of a large-scale gravitational instability comparable to the scale of the model size, 1 LU, if the system velocity dispersion does not exceed some critical value, found to be about 16 km s^{-1}, which is produced by $v_{\rm bst} \simeq 10$ km s^{-1}. (Note that instabilities on smaller scales leading to the formation of gas cloud complexes continue to be present). If the value of $v_{\rm disp}$ is below this critical value the entire matter distribution tends to collapse into a large clump which cannot be dispersed. This critical velocity is closely related to the theoretical stability criterion for a non-rotating sheet consisting of collisionless particles derived by Toomre (1964).

For $v_{\rm bst} < 10$ km s^{-1}, it was found that it was possible to avoid large-scale gravitational clumping by sufficiently reducing the cutoff radius of the force evaluation, which is normally given by $d_{\rm fc} = 0.5$ LU (see subsection 2.2). This effectively reduces the wavelength of the largest possible unstable disturbance. Although in our present simulations we are constrained to admit only simulations with $v_{\rm bst} \geq 10$ km s^{-1} as physically acceptable, this does not mean that smaller values of $v_{\rm bst}$ would not be admissible in models of disc galaxies in which the rotational dynamics work to suppress the growth of gravitational instabilities. An important result is that although the value of $v_{\rm bst}$ affects the systemic velocity dispersion, the global star formation rates and morphology of the star-forming regions are largely unaffected. We furthermore note that for $v_{\rm bst} = 10$ km s^{-1}, the velocity dispersion in local areas temporarily without star formation was found to have a realistic value of around 11 km s^{-1} (measured in areas of size 0.1 LU), a figure significantly smaller than the global (system) velocity dispersion, $v_{\rm disp}$.

In the following subsections we analyze the results produced by simulations run with the set of parameters, $(f_{\rm col}, n_{\rm sp}, n_{\rm st}) = (0.6, 6, 4)$ and $v_{\rm bst} = 10$ km s^{-1}, which we refer to as the 'standard parameter set'. These parameters, with $v_{\rm bst}$ chosen to be equal to the smallest value that does not lead to a global gravitational instability for $d_{\rm fc} = 0.5$ LU, produce simulations satisfying the acceptability criteria described above.

3.2. *Temporal Evolution of the Model*

The number of stellar tracer particles per time step, which is an effective measure of the star formation rate (SFR), and the rms velocity dispersion of the system are

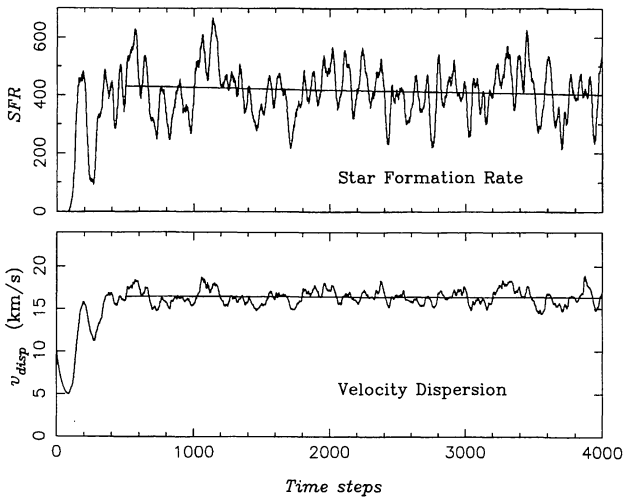

Fig. 2. Time variation of the star formation rate (SFR) and the systemic velocity dispersion ($v_{\rm disp}$) for a 'standard' simulation. The SFR is given by the number of stellar tracer particles per time step, and the velocity dispersion is calculated with respect to the mean x, y velocities of the system. Linear fits to the data for $T > 500$ time steps are shown.

two of the most important global properties describing the evolution of the model. In figure 2 we present the variation of these quantities as a function of time for a simulation run with the standard parameter set for $T = 0$ to $T = 4000$ time steps and show linear fits to the simulation data for $T > 500$ time steps. It can be seen that both quantities exhibit large fluctuations but approach a statistically stationary state before $T \simeq 500$ time steps. Ergodicity is indicated by the fact that linear fits to both sets of data give curves which are nearly flat. In figure 2, the SFR fluctuates by a factor of three, ranging between 215 and 667 stellar tracer particles per time step with a mean and standard deviation of 416 ± 84. The velocity dispersion ranges between 14.4 km s^{-1} and 19.0 km s^{-1} with a mean and standard deviation of 16.4 ± 0.9 km s^{-1}. Interestingly, the SFR trace produced by an SSPSF model for a galaxy with a radius of 3 kpc with a comparable total active area to our model has a similar range in SFR, $\sim$ 3–4, and a similar percentage of surface area undergoing star formation (2–7%) (Gerola et al. 1980).

The peaks of the SFR curve in figure 2 appear to coincide with those of the velocity dispersion curve, which is not surprising since stellar tracer particles are responsible for injecting kinetic energy into the system. The time series were analyzed with the Chaos Data Analyzer (Sprott, Rowlands 1995) and power spectra were examined for the SFR (figure 3) and the velocity dispersion. The power spectra of the two curves were similar, confirming the existence of a close relationship between the SFR and

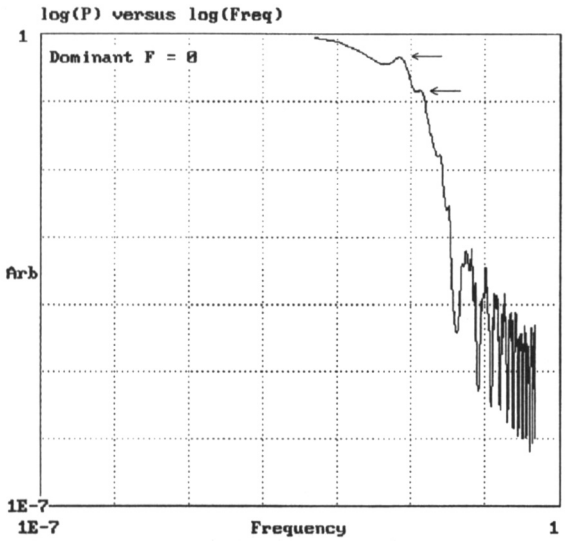

Fig. 3. Power spectrum for the SFR trace shown in figure 2 produced by the 'Dominant Frequencies' routine in the Chaos Data Analyzer program (Sprott, Rowlands 1995). Power (mean square amplitude) in arbitrary units is plotted against frequency in reciprocal time step units in a log–log view. Two peaks corresponding to characteristic periods of 150 and 75 time steps superimposed on a continuous spectrum are indicated by arrows.

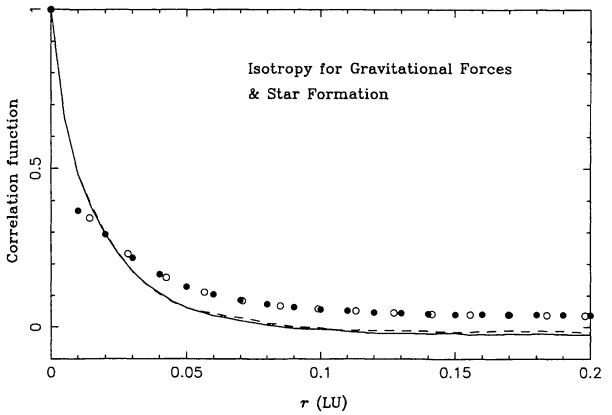

Fig. 4. Correlation functions for gravitational forces and star formation generated to test isotropy. The correlation functions for gravitational forces are denoted by solid (rectilinear direction, i.e., average of $\theta = 0°, 90°$) and dashed (diagonal direction, i.e., average of $\theta = 45°, 135°$) curves. The correlation functions for star formation are indicated by filled (rectilinear direction) and open (diagonal direction) circles. See text for details.

the velocity dispersion. Two peaks, representing dominant frequencies corresponding to periodicities of 150 and 75 time steps, are superposed on a continuous background curve which falls to essentially zero amplitude at a minimum periodicity of 35 time steps. This indicates that quasiperiodic fluctuations in the SFR occur on a range of timescales longer than about 20 Myr and that two characteristic timescales of 75 Myr and 37 Myr exist which appear to be related to the natural period of oscillation associated with the creation and destruction of individual star-forming cloud complexes. The magnitudes and timescales of the SFR and velocity dispersion fluctuations suggest that star formation in galaxies where self-propagating star formation is important is far from being a steady-state phenomenon.

3.3. Isotropy

To investigate any dependence of the properties of the simulations on the square geometry of the CA grid applied for star formation, we determined two-point correlation functions for (a) gravitational forces, and (b) star formation, for the rectilinear and diagonal directions defined relative to the edges of the square model surface. We defined a normalized two-point correlation function, $CF(r,\theta)$, centred on a point (x_o, y_o) for a property, $P(x,y)$, as

$$CF(r,\theta) = \frac{\overline{P(x_o,y_o)\,P(x_o+r\cos\theta, y_o+r\sin\theta)}}{[\overline{P(x_o,y_o)^2}]^{\frac{1}{2}}\,[\overline{P(x_o+r\cos\theta, y_o+r\sin\theta)^2}]^{\frac{1}{2}}}, \quad (6)$$

where the averages are taken over time. The correlation function is calculated as a function of distance, r, from (x_o, y_o) for a given direction specified by an angle, θ, measured anti-clockwise from the x-axis. Assuming ergodicity, and sampling a sufficient number of points (x_o, y_o), we would demonstrate perfect isotropy if the correlation functions for different values of θ were identical.

Isotropy for gravitational forces and star formation was tested by determining $CF(r,\theta)$, for $\theta = 0°, 90°, 45°$, and 135°. In the case of gravitational forces, $P(x,y)$ was given by the component of the force directed along the θ direction, $F_\theta(x,y)$. Isotropy for star formation was tested using a property, $s(x,y)$ with possible values $s = 0, 1$, derived from the association of stellar tracer particles with 0.01 square LU star-forming cells having centres (x,y). The time averages were taken over 1000 time steps sampled every fifth time step and sufficient spatial sampling was used to generate smooth correlation functions.

The resulting correlation functions, displayed in figure 4, convincingly demonstrate the existence of almost perfect isotropy for both gravitational forces and star formation. For the star formation plot, the data point for the first diagonal cell would lie only slightly above a straight line joining the first and second rectilinear data points and the agreement is excellent thereafter. Thus the propagation of star formation is almost

completely isotropic, a result which appears to be consistent with patterns of propagating star formation observed in 2D plots of the cloud particle and stellar tracer particle distributions (see section 4).

3.4. *Global Energetics*

Here we determine the mean rate of injection of kinetic energy produced by stellar tracer particles in our model and compare it with the energy released by supernovae in the Large Magellanic Cloud (LMC), an irregular galaxy with an active area of star formation comparable to our system. This comparison is essential for investigating whether our model can realistically represent the output of energy from star-forming regions. We first determine the equivalent number of supernova events per time step represented by a single active stellar tracer particle. The supernova rate in the LMC is one per 240 yr (Long et al. 1981), giving $\sim$ 2000 supernova events occurring in 0.5 Myr, equivalent to one time step in our model. The number of active stellar tracer particles per time step in a 'standard' simulation is $\sim$ 400, so a single stellar tracer particle should represent approximately 5 supernova events per time step. The kinetic energy released by a single supernova explosion is of the order of 10^{51} erg. We thus obtain an equivalent energy release rate per stellar tracer particle of 5×10^{51} erg per 0.5 Myr, or 3.1×10^{38} erg s^{-1}.

We now compute the actual mean rate of kinetic energy input per active stellar tracer particle using simulation data covering a period of 200 time steps. Simulation data were recorded which enabled the calculation of precise amounts of kinetic energy loss by collisional dissipation and of kinetic energy gain from boosting by stellar tracer particles. The changes in kinetic energy were measured only in regions affected by star-forming activity. We measured the total gain in kinetic energy in 0.01 LU square cells possessing particles which actually received boosts from stellar tracer particles, and also the total loss in kinetic energy in these same cells as a result of collisional dissipation. The number of stellar tracer particles giving boosts to nearby particles was counted and it was found that only about 1% of the active stellar tracer particles had no cloud particles within the maximum boost radius. In this way, a mean energy injection rate per stellar tracer particle of 2.3×10^{36} erg s^{-1} was obtained after subtracting out the kinetic energy loss through collisional dissipation. (The kinetic energy gain from the boost phase in star-forming regions was almost exactly twice the kinetic energy loss through collisions.) Thus the ratio of the actual energy injection rate to the equivalent energy release rate per stellar tracer particle is $2.3 \times 10^{36}/3.1 \times 10^{38} = 0.0074$. This represents an efficiency of conversion of the energy from supernovae into kinetic energy of the interstellar medium of 0.7%. This figure is of the same order of magnitude as the 1.7% efficiency for LMC Shapley Constellation III implied by Dopita, Mathewson, and Ford (1985), for energy release from supernovae $\simeq 5 \times 10^{39}$ erg s^{-1} over 15 Myr and kinetic energy of the expanding H I shell of 4×10^{52} erg. Thus the global energetics produced by our model are clearly consistent with the total output of energy from supernovae events.

4. Simulation Results — Local Structure

We now examine the detailed distribution of gas cloud particles and stellar tracer particles in order to understand the spatio-temporal evolution of gaseous structures and star formation depicted in our model. We present, in figures 5a,b, six evolutionary snapshots of the gas cloud and stellar tracer particle distributions covering a period of 25 Myr from T = 750–775 Myr (1500–1550 time steps), the interval between successive frames being equal to 5 Myr (10 time steps). The total star formation rate increases from about 300 stellar tracer particles per time step at T = 750 to 500 at T = 775 Myr. The birth, expansion and dissolution of star-forming structures is clearly shown in these plots, which represent the typical behaviour of the model at other times. Cloud complexes consisting of around 100–150 particles with linear dimensions of around 0.06 LU (300 pc) are frequently formed as a result of local gravitational instabilities enhanced by collisional cloud cooling in areas temporarily without star formation activity. We chronicle the evolution of one such structure located at around (0.4, 0.3):

(A) T = 0 (time steps + 1500): a cloud complex has formed at this location but has yet to begin forming stars.

(B) T = 10: the complex has contracted sufficiently for star formation to be ignited in the central part and four stellar tracer particles have appeared.

(C) T = 20: star formation has propagated through the complex with the appearance of 19 stellar tracer particles, and a central cavity has begun to appear created by the kinetic boosts from the stellar tracer particles.

(D) T = 30: the 'shell' of gas particles has expanded considerably to a linear size of 0.14 LU (700 pc).

(E) T = 40: The gas structure is becoming more dispersed, with the remnants of star formation activity located in a disconnected ring-like structure.

(F) T = 50: The gas structure is well on its way to complete dissolution into the ambient interstellar medium.

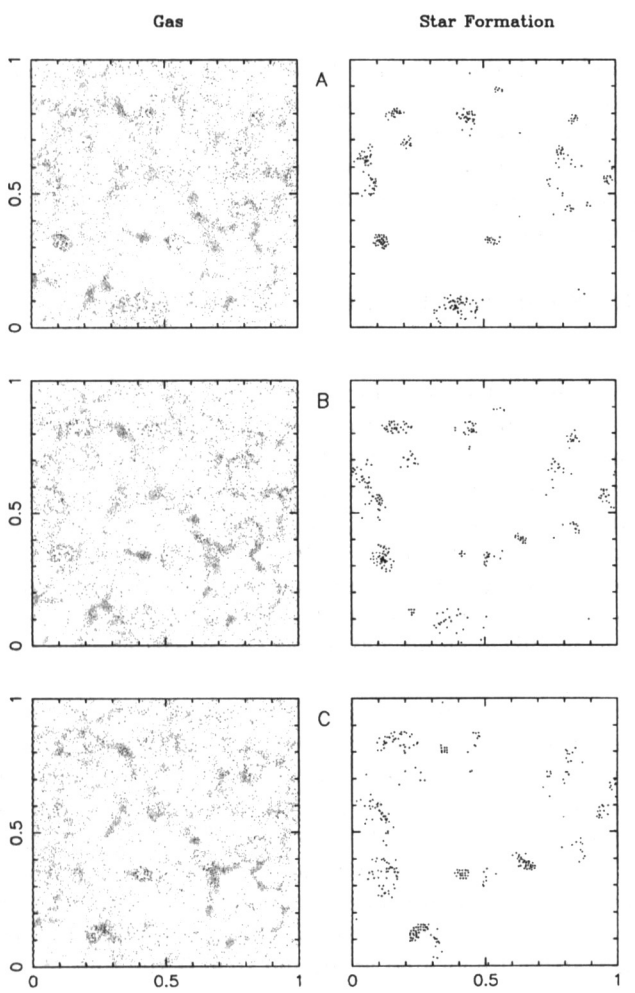

Fig. 5a. Evolutionary snapshots of the gas cloud (left) and stellar tracer particle distributions (right) produced by a 'standard' simulation. The total period covered in figures 5a,b (frames A–F) is 25 Myr from $T = 750$–775 Myr (1500–1550 time steps), the interval between successive frames being equal to 5 Myr (10 time steps). Frames A (750 Myr), B (755 Myr), C (760 Myr) are shown.

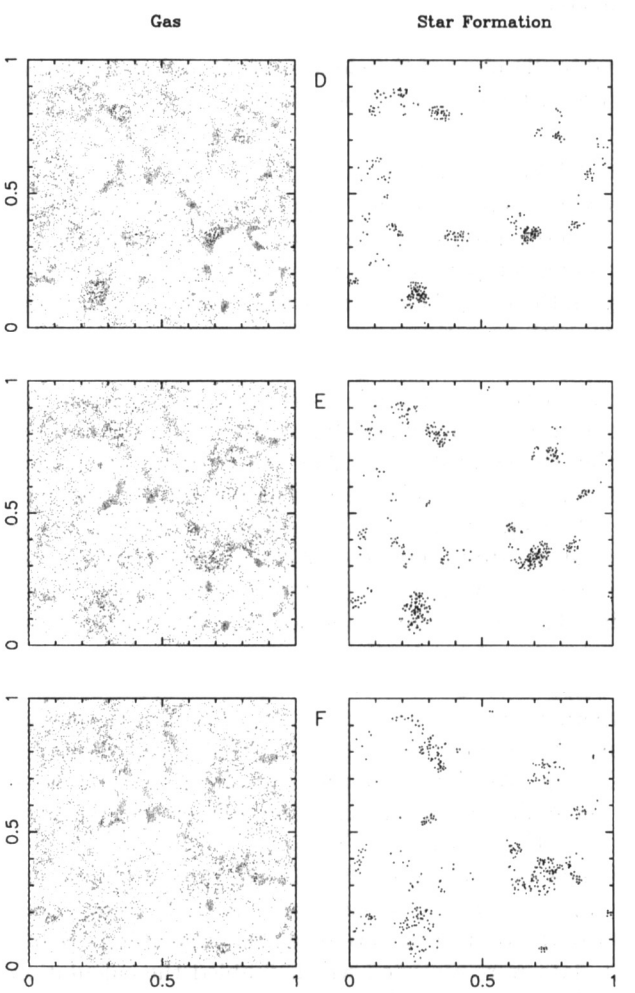

Fig. 5b. Continued evolution of gas cloud (left) and stellar tracer particle distributions (right) depicted in figures 5a (A–C), frames D (765 Myr), E (770 Myr), F (775 Myr) are shown.

All or part of this scenario is enacted by several other structures, including those at (0.3, 0.2), (0.6, 0.4), (0.6, 0.5), (0.4, 0.8), (0.5, 0.3), (0.7, 0.1), and (0.1, 0.3). We thus find that shells of gaseous material enclosing low density bubbles are naturally generated by star-forming activity and gas cloud dissipation in the model, giving rise to expansion velocities of around 10–20 km s^{-1}. Star formation propagates outwards from the central point of ignition at the core of the cloud complex, but gradually dies out as the shell disperses. In the Magellanic Clouds, the interstellar medium contains numerous low-density holes surrounded by H I shells according to high resolution observations by Kim et al. (1997) and Staveley-Smith et al. (1997). The scenario of star formation propagating from the centre to the periphery of a cloud complex, generating an expanding shell of H I is supported by observations of Shapley Constellation III in the LMC (Dopita et al. 1985), and the study of the supergiant shell LMC 2 by Caulet et al. (1982) also suggests the existence of a high velocity expanding gaseous shell driven by the combined action of stellar winds and supernovae.

The masses and radii of the cloud complexes which form in our model, ~ 6–$9 \times 10^6\,M_\odot$, are comparable to those measured for giant molecular clouds in the LMC by Cohen et al. (1988). The virial masses of most of the molecular clouds range between $\sim$ 1–$9 \times 10^6\,M_\odot$. The radii of these clouds are between 100–300 pc compared to a typical complex radius of $\sim$ 150 pc in our model. By examining snapshots covering a longer time span than depicted in figure 5, we found that a typical timescale for cloud complex formation from a fairly

uniform background until the onset of star formation is around 40–50 Myr. For comparison, the theoretical calculations of Elmegreen (1989) involving gravitational instabilities in a cloudy interstellar medium give timescales for the formation and collapse of gas cloud complexes (in conditions similar to the solar neighbourhood) of between 40 to 100 Myr depending on the masses of the structures formed, ranging from 6×10^5–$6 \times 10^7\ M_\odot$.

5. Discussion

In this section, we discuss our model in relation to the models of Stochastic Self-Propagating Star Formation (SSPSF), and the possibility of simplifying our model by neglecting inter-particle gravitational effects.

First, we obtain some statistical results of our simulations with reference to the SSPSF models developed by Gerola, Seiden, and coworkers (e.g., GS78; Seiden et al. 1979). These models represent a type of probabilistic cellular automaton implemented on a specialized geometry for simulating the propagation of star formation in rotating disc galaxies. In spite of the heuristic and mainly statistical nature of these models, they were strikingly successful in reproducing spiral patterns of star formation in multi-armed spiral galaxies, convincingly demonstrating that large-scale order could result from the purely local process of propagating star formation. The implementation of the star formation process in our model has some similarities to the SSPSF code, and we might expect our model to manifest some similar statistical behaviour.

The models of SSPSF are based on the assumption that star formation in galaxies is dominated by stimulated processes, with spontaneous star formation playing a rather minor role. In our own model, such an assumption is implicit in the positing of different particle density thresholds for stimulated and spontaneous star formation, with $n_{\rm st} < n_{\rm sp}$. We now show that for simulations run with standard sets of parameters, our model and the SSPSF models produce similar rates for the ratio of stimulated to spontaneous star formation. First, we state that the duration of a star formation event (lifetime of a stellar tracer particle) in our model, 12 Myr, is similar to that in the SSPSF model of Gerola and Seiden (GS78), namely 15 Myr, allowing us to compare directly the percentages of star-forming cells in the two models. For our model, about 4% of model area is active in the mean, while in the model of GS78, the figure is 2%. We ran simulations which recorded the numbers of stellar tracer particles formed per timestep by spontaneous and stimulated modes, and found that the ratio of stimulated to spontaneous star formation was ~ 100. The probability for spontaneous star formation per cell per time step, $P_{\rm sp}$, in the SSPSF models was typically 0.0002, although the generation of good spiral features was rather insensitive to this parameter. In other words, 0.02% of the total area of the model galactic disc will undergo spontaneous star formation in one time step. This gives a ratio of stimulated to spontaneous star formation activity of ~ 100, the same value which emerges in our model. We point out that different ratios would be obtained for SSPSF models having different values of $P_{\rm sp}$, and also for different values of the threshold parameters for star formation in our model. Nevertheless, our results indicate a remarkable consistency between these two otherwise disparate models.

An intriguing question to ask is whether all the physical detail contained in the present model is actually necessary to simulate the global spatio-temporal evolution of star formation in galaxies, or whether a simpler model might reproduce qualitatively similar results. To this end, we have also examined the possibility of simplifying the current model, and thereby greatly reducing the computational overhead, by omitting inter-particle gravitational forces altogether. Such a numerical scheme is equivalent to a random collisional buildup model, in which the gravitational forces are considered to be essentially inoperative and agglomeration into large cloud complexes occurs solely by the sticking effect of random collisions. We conducted a number of trial simulations with gravity turned off in order to find combinations of parameters which gave simulations with comparable levels of star formation activity compared to the results of the gravitational simulation ran with a standard set of parameters, i.e., (0.6, 6, 4), $v_{\rm bst} = 10$ km s^{-1}. In particular, the elasticity parameter, $f_{\rm col}$, was reduced to its lowest possible value to enhance the sticking effect of random collisions. A simulation without gravitational forces with a set of parameters (0.0, 5, 4), $v_{\rm bst} = 5$ km s^{-1}, was found to reach stationarity with an average star formation activity level of approximately 400 stellar tracer particles per time step. A series of snapshots of the simulation covering a period of 10 Myr is shown in figure 6.

When compared to a typical gravitational simulation (see figure 5), several differences are noted. The most obvious is the reduced level of clumping seen in the non-gravitational model which tends to give rise to more dispersed star formation activity. Elmegreen (1990) has shown analytically that the mechanism of gravitational instability leads to the formation of cloud complexes at rates approximately three times greater than random collisions. The lower rate of clump formation in the non-gravitational model, even with $f_{\rm col} = 0.0$, is confirmed by additional trial simulations with star formation also turned off, showing that gravitational forces lead to the formation of clumps on timescales at least 3–4 times shorter than in the absence of gravity. In the non-gravitational model with star formation, the reduction in clumping is partially compensated by a lower spontaneous star formation threshold to give an equivalent level of star formation activity. Examining figure 6

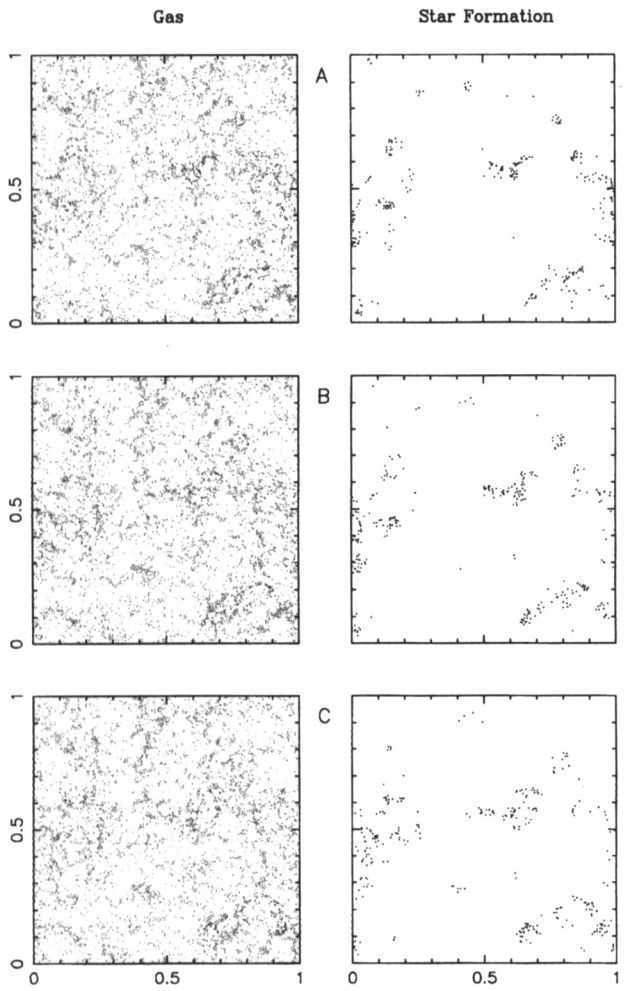

Fig. 6. Non-gravitational model including star formation. Snapshots of the gas cloud (left) and stellar tracer particle distributions (right) produced by a simulation without particle self-gravity. The period covered is 10 Myr from T = 785–795 Myr (1570–1590 time steps), the interval between successive frames being equal to 5 Myr (10 time steps)

again, the presence of expanding shells of star formation activity is also recognizable; however, such features are not as clearly defined as in the gravitational model. For models of galaxies with a spiral density wave (e.g., Roberts, Hausman 1984), the spiral potential should enhance the clumping, and a model without explicit interparticle gravitational interactions may then be sufficient to describe the star formation activity. In general, however, we consider the inclusion of gravitational forces an important aspect for modelling the formation of cloud complexes with realistic internal structure for the superposition of the star formation process.

6. Adaptation to Disc Galaxies

As mentioned previously, we aim to apply the simulation code to the case of rotating disc galaxies and such work is currently proceeding. We had previously comtemplated the possibility of employing a polar grid such as is used in the SSPSF models of disc galaxies. However, such geometrical modifications to the present model would appear to be unnecessary in the light of the results of our isotropy tests (subsection 3.3). The propagation of star formation has been demonstrated to be almost completely isotropic and therefore the current scheme based on square star-forming cells should be adequate. Furthermore, any residual anisotropy could conceivably be eliminated by rotating the underlying square grid for the star-forming cellular automaton scheme by a *random* angle relative to the particle distribution at each time step since the stellar tracer particles exist independently of the grid after they have formed. Although square cells are employed to determine the ignition of star formation, the basic unit representing newly created stars is not the star-forming cells, which are fixed in space, but the stellar tracer particles, which can move ballistically in the local gravitational field. Thus, in a disc galaxy, the stellar tracer particles and the range of influence associated with them rotates with the rest of the matter distribution about the galactic centre.

We aim to apply our numerical code to models of rotating disc galaxies (namely, spiral, dwarf and irregular galaxies) in order to investigate the generation of patterns of star formation and thereby determine to what extent the process of propagating star formation can lead to the production of both large- and small-scale star-forming structures.

The authors would like to thank the Sun Moon University Research Centre for financial assistance for this work. We would also like to thank Dr. M. Noguchi (Tohoku University) and the anonymous referee for helpful comments on the manuscript.

References

Barnes J., Hut P. 1986, Nature 324, 446
Bouchet F.R., Hernquist L. 1988, ApJS 68, 521
Braunsfurth E., Feitzinger J.V. 1983, A&A 127, 113
Bruhweiler F.C., Gull T.R., Kafatos M., Sofia S. 1980, ApJ 238, L27
Caulet A., Deharveng L., Georgelin Y.M., Georgelin Y.P. 1982, A&A 110, 185
Cohen R.S., Dame T.M., Garay G., Montani J., Rubio M., Thaddeus P. 1988, ApJ 331, L95
Domgörgen H., Bomans D.J., de Boer K.S. 1995, A&A 296, 523
Dopita M.A., Mathewson D.S., Ford V.L. 1985, ApJ 297, 599
Dubinski J. 1996, New Astron. 1, 133

Elmegreen B.G. 1989, ApJ 344, 306
Elmegreen B.G. 1990, ApJ 357, 125
Elmegreen B.G.M., Thomasson M. 1993, A&A 272, 37
Feitzinger J.V., Glassgold A.E., Gerola H., Seiden P.E. 1981, A&A 98, 371
Gerola H., Seiden P.E. 1978, ApJ 223, 129 (GS78)
Gerola H., Seiden P.E., Schulman L.S. 1980, ApJ 242, 517
Hausman M.A., Roberts W.W.Jr 1984, ApJ 282, 106
Hernquist L. 1987, ApJS 64, 715
Hunter D.A. 1982, ApJ 260, 81
Kim S., Freeman K.C., Staveley-Smith L., Sault R.J., Kesteven M.J., McConnell D. 1997, PASA 14, 119
Kojima M., Noguchi M. 1997, ApJ 481, 132
Lejeune A., Perdang J. 1996, A&AS 119, 249
Long K.S., Helfand D.J., Grabelsky D.A. 1981, ApJ 248 925
Luks Th., Rohlfs K. 1992, A&A 263, 41
Mihos J.C., Hernquist L. 1994, ApJ 437, 611
Navarro J.F., White S.D.M. 1993, MNRAS 265, 271
Noguchi M. 1988, A&A 203, 259
Noguchi M. 1991, MNRAS 251, 360
Noguchi M., Ishibashi S. 1986, MNRAS 219, 305
Perdang J., Lejeune A. 1996, A&AS 119, 231
Reid N., Mould J., Thompson I. 1987, ApJ 323, 433
Roberts W.W., Hausman M.A. 1984, ApJ 277, 744
Seiden P.E., Gerola H. 1979, ApJ 233, 56
Seiden P.E., Schulman L.S., Gerola H. 1979, ApJ 232,702
Sleath J.P., Alexander P. 1995, MNRAS 275, 507
Smith A.M., Cornett R.H., Hill R.S. 1987, ApJ 320, 609
Sprott J.C., Rowlands G. 1995, Chaos Data Analyzer (Professional Version), Physics Academic Software (AIP, New York)
Staveley-Smith L., Sault R.J., Hatzidimitriou D., Kesteven M.J., McConnell D. 1997, MNRAS 289, 225
Tissera P.B., Lambas D.G., Abadi M.G. 1997, MNRAS 286, 384
Toomre A. 1964, ApJ 139, 1217
Turfus C., Gardiner L.T. 1996, Trans. Cent. Sci. Technol. (Sun Moon University, Asan, Korea) 1, 98